EXPERIMENTAL AND CFD ANALYSIS OF MHD FLOW AROUND SMOOTH SPHERE AND SPHERE WITH DIMPLES IN SUBCRITICAL AND CRITICAL REGIMES

by

Jasmina B. BOGDANOVIĆ-JOVANOVIĆ and Živojin M. STAMENKOVIĆ [*]

Faculty of Mechanical Engineering, University of Nis, Nis, Serbia

Original scientific paper
https://doi.org/10.2298/TSCI200430197B

An overview of previous researches related to the problem of flow around a bluff-body, using experimental and numerical methods, is presented in the paper. Experimental investigation was performed by a laser doppler anemometer, measuring velocity components of the water flow around a smooth sphere, and a sphere with dimples in square channels. Measurement results in subcritical velocity flow field, velocity fluctuation components, lift, drag and pressure coefficients, and 2-D Reynolds stress at quasi-stationary flow are conducted using 1-D laser doppler anemometer probe. The obtained experimental results are compared with numerical simulations, which are performed using the ANSYS-CFX software. For the numerical simulations of quasi-steady-state flow, k-ω turbulent model was used, while for numerical simulation of unsteady fluid-flow and for the comparison of results related to the eddy structures, vortex shedding and Reynolds stresses, detached eddy simulation were used. Since the obtained results of experimental and numerical investigation of flow around smooth sphere and sphere with dimples showed good agreement, the considered flow problem was expanded by introducing the influence of a transverse magnetic field with a slight modification of the electrical conductivity of the working fluid. The other physical properties of the fluid remained the same, which also corresponds to realistically possible physical conditions. Numerical simulations were performed for three different values of Hartmann number and very small values of Reynolds magnetic number (inductionless approximation). Comparisons and analyzes of the results were made for the cases containing a magnetic field and those with an absence of a magnetic field.

Key words*: fluid-flow, bluff body, velocity, magnetic field, MHD*

Introduction

Researches in the field of MHD began in the early 19th century with a Faraday experiment, indicating the mutual interaction of the Earth's magnetic field and the movement of conductors (the Thames River). Also, Ritchie experimentally demonstrated that fluids could be driven by electromagnetic forces. However, the development of theoretical and applied MHD really began in the 1930's. For some authors, the beginnings of MHD are related to Hartmann and Lazarus and their experiments in 1937's. There are also other opinions that the founder of these studies was Alfven, who discovered that the interaction of electrically conducting fluid

[*] Corresponding author, e-mail: zivojin.stamenkovic@masfak.ni.ac.rs

and magnetic field leads to the formation of waves named after him as Alfven's waves (in 1942's).

The engineering and industrial application of MHD research first appeared in metallurgy in the early 1960's with the aim of increasing process efficiency and product quality. The first electromagnetic pumps are used for the transport of liquid metals, for mixing a metal solution using rotating magnetic fields, to obtain more homogeneous structures, and static magnetic fields are applied in the prevention of surface contamination. Further development of the technique enabled the application of MHD in the field of controlled growth of silicon crystals, as well as application in the development of non-invasive flow measurement techniques (magnetic-flow meters and Lorentz force velocimetry).

Nowadays, the phenomena of a magnetic field and conductive fluid interaction find their application in micro-fluidics, biomedicine, fusion reactor cooling systems, ship propulsion, turbulence reduction, filtration and separation. The MHD pumps represent alternatives to centrifugal pumps, especially when transporting liquid metals and aggressive fluids due to the absence of moving parts and significantly increased reliability, which is their key advantage. It should be emphasized the current application of MHD in biological fluids such as blood, magnetic targeting of drugs and immunomagnetic cell separation. Nowadays micro-fluidic devices are used in drug dosing, fluid mixing or transport, and in recent years there has been an increasing interest in applications in chromatography and DNA replication.

In many MHD applications, there are cases of fluid-flow around non-conducting bodies, which are placed inside the flow domains. Note that such non-conducting objects do not directly suffer from magnetic forces, but as there is an interaction between the electrically conducting fluid and the magnetic field, there is also an indirect influence between the body and the fluid.

The primary motive for conducting this study is to analyze the effect of a magnetic field on flow around a bluff body in laminar and turbulent flow regimes with the high value of blockage factors. The application of a strong magnetic field perpendicular to fluid-flow leads to laminarization of the fluid-flow, since velocity fluctuations in the direction of a magnetic field are strongly absorbed. This phenomenon is often used in engineering applications to change the properties and mechanisms of heat and mass transfer.

On the other hand, eddy structures with axes parallel to the applied magnetic field are not significantly reduced, and this phenomenon is used in technical practice to intensify heat transfer by using a turbulence promoter such as, placing a circular cylinder in a channel.

Fluid-flow around bluff body always depends on the Reynolds number, but the question of whether the ratio of viscous and inertial forces is the only influential factor depends on whether the body is in a bounded or unbounded flow domain. For unbounded flow domains, the only influential parameter is the Reynolds number, while for bounded flow domains, another influential parameter is commonly known as the blockage ratio (ratio of sphere projection area to channel area). The influence of this parameter on the flow stability and flow parameters, such as thrust and drag coefficients, Nusselt and Strouhal numbers have been considered by several authors: Coutanceau and Bouard [1], Cliffe and Tavener [2], Behr *et al.* [3], Zovatto and Pedrizzetti [4], Anagnostopoulos *et al.* [5], and Sahin and Owens [6]. Experimental investigation of flow around the sphere, for different Reynolds numbers, is conducted by Bakić *et al.* [7], giving emphasis to turbulent structures and flow visualization.

In the case of MHD flow around the bluff body, there are additional control parameters that can change the flow field. These parameters are expressed through the ratio of electromagnetic and viscous forces (Hartmann number) and the ratio of electromagnetic and inertial forces (interaction parameter). The influence of the magnetic field on the fluid-flow around the circular cylinder and sphere has been discussed by: Haverkort and Peeters [8], Dousset and Pothherat [9], Muck *et al.* [10], Frank *et al*. [11], and experimentally by Alboussiere *et al.* [12]. One of the first researches in this area was given by Kolesnikov and Tsinober [13], who discussed the basic properties of the mentioned flows, while Moreau and Sommeria [14] considered turbulent fluid-flow in a strong magnetic field.

In addition the mentioned methods that can affect the flow around the bluff body, there are other ways that can modify the velocity flow field, such as shaping the surface of the bluff body or suction of fluid. Nowadays, a special attention is given to researches related to active flow control, which is presented as the formation of active dimples. Many researchers today work on the development of the so-called smart surfaces with active depressions that can be modified as needed to control the flow field. The flow control was investigated Dearing *et al.* [15], followed by Lienhart *et al*. [16], who were investigated reducing the drag coefficients by dimples. Also, Luo *et al*. [17] provided an analysis and overview of surface change technologies to reduce drag, while recently Ge *et al.* [18] presented the results of an investigation of active dimples in a wall bounded incompressible turbulent flow.

All the previous studies have motivated the authors of this paper to begin a study of fluid-flow around the bluff body, both experimentally and numerically (CFD), in order to examine the effects of the magnetic field on the flow around the bluff body with high values of the blockage factor. The aim of the study is to experimentally test laminar and turbulent flow regimes around a smooth sphere and a sphere with dimples, for different values of Reynolds number, then to compare the results with numerical results and to validate turbulent models. The main aim of this paper is to compare experimental results obtained by laser Doppler anemometer (LDA) measurements with stationary and non-stationary numerical simulations of flow and to determine the reliability and validity of the model for considering such flow problems in engineering practice.

Selected CFD approaches in conducted analysis include the application of k-ω turbulent model for stationary flow simulations, since it gave the best results in earlier studies of flow around bluff bodies [19]. For non-stationary fluid-flows a detached eddy simulation (DES) approach was used, where the production member is modified compared to the original RANS models. In the fluid-body contact zones it switches to the RANS model, while the LES model is applied further away from the walls.

Another set objective of this research is to extend the used CFD models by introducing the effect of a transverse magnetic field and fluid conductivity, and to use the obtained results to draw general conclusions about the influence of the magnetic field on the flow characteristics, while keeping all other parameters the same to ensure the proper hydrodynamic similarity.

Problem description

The previously conducted studies included an experimental part related to LDA measurements around the smooth sphere, where the blockage factor is 0.223, and the sphere with dimples, where the blockage factor is 0.133.

For the purposes of these investigations, standard square channels of external dimensions 80 × 80 (inner 75 × 75) and 100 × 100 (inner 92.5 × 92.5) are used. A ping-pong and a golf ball, which is slightly smaller than a standard golf ball, are used as bluff bodies.

The fig. 1 shows both flow domains in which LDA measurements were conducted.

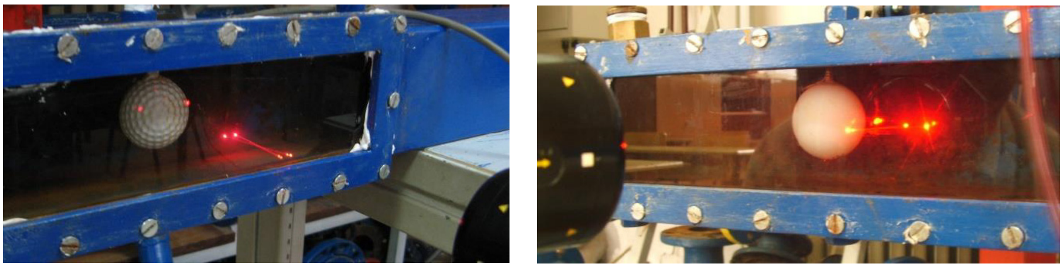

Figure 1. A sphere with dimples and a smooth sphere during the LDA measurements

The dimensionless values that characterize the considered flow regimes, in both experimental and numerical (CFD) investigations, are defined by the diameter of the sphere in the channel, such as: Reynolds number, blockage factor, drag coefficient, lift coefficient, pressure coefficient, Hartman number, interaction parameter, and Reynolds magnetic number. There are defined by the following expressions:

$$\mathrm{Re}=\frac{u_{ave}d_{sp}}{\nu},\quad \beta=\frac{\dfrac{d_{sp}^2\pi}{4}}{b_{\mathrm{channel}}^2},\quad y^*=\frac{y}{b_{\mathrm{channel}}},\quad z^*=\frac{z}{b_{\mathrm{channel}}},\quad c_d=\frac{2F_d}{\rho u_{ave}^2\dfrac{d_{sp}^2\pi}{4}}=\frac{8F_d}{\rho u_{ave}^2 d_{sp}^2\pi}$$

$$c_l=\frac{2F_l}{\rho u_{ave}^2\dfrac{d_{sp}^2\pi}{4}}=\frac{8F_l}{\rho u_{ave}^2 d_{sp}^2\pi},\quad c_p=\frac{p-p_{in}}{\dfrac{1}{2}\rho u_{ave}^2},\quad \mathrm{Ha}=Bd_{sp}\sqrt{\frac{\sigma}{\mu}},\quad N=\frac{\sigma B^2 d_{sp}}{\rho u_{ave}},\quad \mathrm{Re}_m=u_{ave}d_{sp}\sigma\mu_0$$

For all later analysis, graphs and results presentations, it is assumed that the flow is in the direction of x-axis, and velocity component in this direction is denoted by the letter u. The y-axis is parallel to the applied magnetic field and the velocity in that direction is denoted by the letter v. The z-axis is transverse to the flow and magnetic field. Asterisks refer to dimensionless values as defined in expressions (1).

The smooth sphere is 40 mm in diameter, d_{sp}, and it is placed in a smaller quadratic duct, while the sphere with dimples is 38 mm in diameter, also d_{sp}, and it is placed in a larger quadratic duct.

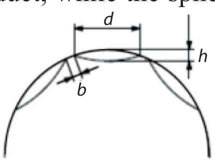

Figure 2. Sphere with dimples

The basic dimensions of the sphere with dimples, used in our experimental and numerical investigations, are shown in fig. 2. Dimples are inward semi spherical shaped, where the dimple width is d = 3.5 mm, the depth of dimple is h = 0.4 mm and the distance between dimples is b = 0.4 mm.

Measurements of the incoming flow velocity field were conducted in a measuring window located before the main measuring window (where measurements around spheres were conducted). The experimental facility also includes a magnetic-flow meter, which is installed to perform a constant check of the steady-state flow regime, *i.e.* velocity flow rate value during the measurements. These measurements were performed for several reasons: the first is to determine the existence of a uniform velocity field of the incoming flow in the channel, before the sphere; the other reason is to form an inlet velocity profile for CFD simulations, thereby significantly reducing the considered flow domain.

The intensity of turbulence was measured for different turbulent flow regimes, and the intensity of free-flow turbulence was determined in the range of 3-5%.

During the measurements, in many sections in front of the spheres, two velocity components were measured: longitudinal u and transversal v, as well as their fluctuations. Measurements of the 2-D Reynolds stress tensor of a steady or periodic flow were made using a rotated 1-D probe instead of a 2-D LDA system, showing respectable results for a lower investment cost of measuring equipment [20].

A part of the experimental research presented in the paper relates to the following values of Reynolds numbers:

– for a smooth sphere Re = 1300, Re = 16000,
– for a sphere with dimples Re = 1000, Re = 10000 and Re = 20000

As previously mentioned, to obtain as many identical conditions as possible for performing numerical analyzes, which are later compared with the experimental results, the velocity and turbulence fields of the free incoming undisturbed fluid-flow were measured. The measured velocity field was used to determine the actual mean velocity in the channel and to determine the Reynolds number of the tested flow regime, and on the other hand was used in the preparation of CFD simulations by defining the velocity field as a matrix of the velocity field at the inlet of the flow domain. In this way it is possible to reduce the considered flow domain and to create a considerably finer finite volume mesh used for CFD analyze, whereby the time required to obtain a given accuracy is significantly reduced.

In analyzing the influence of the magnetic field on the considered flow problem, the values of the magnetic field intensity were determined such that the previously defined Hartmman number takes values 8, 25, and 50, when Reynolds magnetic number is of the order 10^{-8}, while the interaction parameter N is of the order 10^{-2} to 10^{-1}, and it can be easily determined for each case based on given data.

In order to obtain better numerical results, very fine unstructured tetrahedral meshes were created with prismatic elements on the walls and around the sphere surface. The number of mesh elements for both meshes, a smooth sphere mesh and a sphere with dimples, are around 5 million. Figure 3 shows the correspondent cross-sections of created discretization meshes. Number of prismatic layers around the spheres are 25, where initial element height is 0.001, with the height ratio 1.2.

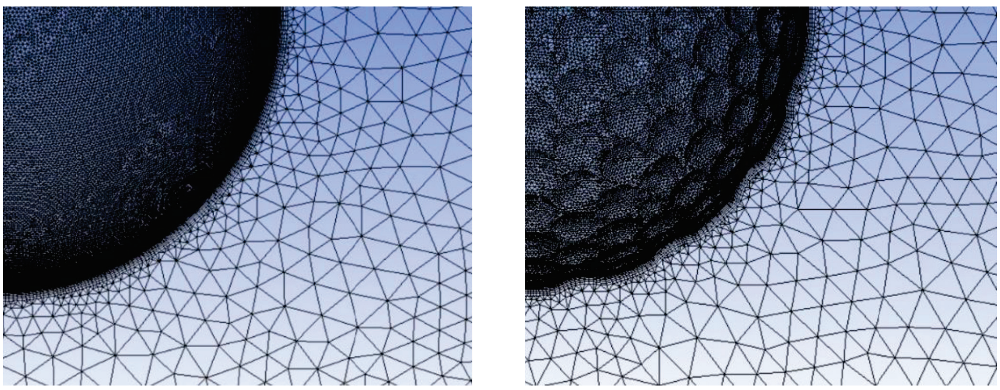

Figure 3. Discretization meshes in the flow domain (smooth and sphere with dimples)

The usual procedure for choosing an adequate mesh is to perform a mesh independence test. Despite the obtained results, which indicate the possibility of using coarser meshes, the finer meshes with around 5 million elements were chosen, since the reduction of the flow domain enables the use of better-quality mesh, while at the same time the computational time necessary to perform numerical simulations remains satisfactory small.

Experimental and CFD results

After extensive measurements and CFD simulations (steady and transient), the results obtained were compared and analyzed, and part of the results are shown in the following graphs. In graphical presentation of the results, the cross-sections in which the comparisons of the results are made are defined in the axis of the channel and the distance, L, is defined with respect to the axis of the sphere. Both distances and velocities are given in dimensionless form.

Velocity profiles of flow around the smooth sphere, obtained experimentally and numerically for flow regime (Re = 1300), are presented in fig. 4. The influence of the magnetic field on the velocity profiles in several different cross-sections is given for Ha = 8, 25, and 50.

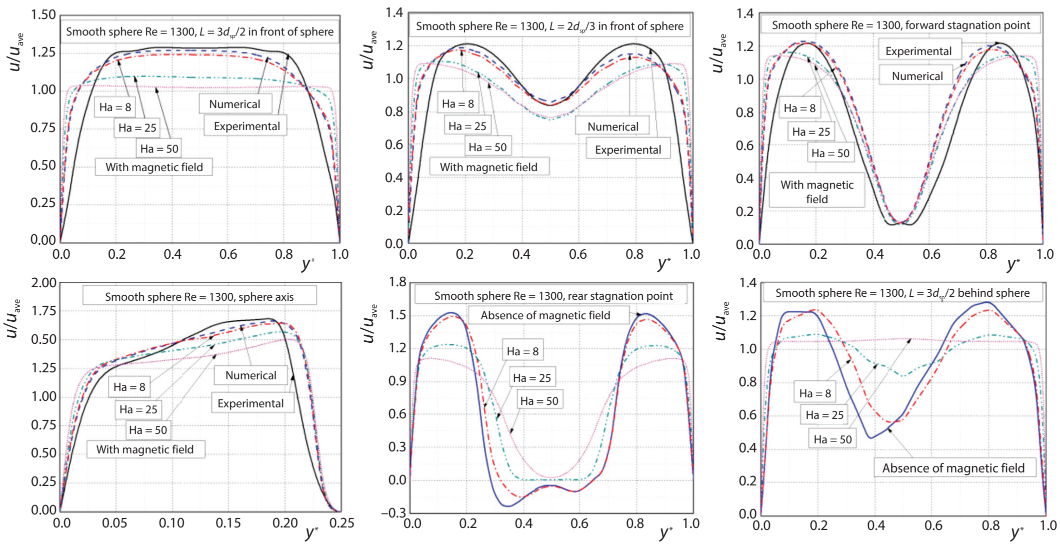

Figure 4. Comparison of velocity profiles for flow around the smooth sphere (Re = 1300)

First, it is important to note the very good agreement between the CFD and experimental results, obtained using LDA measurements. Experimental results indicate *more laminar* velocity profile, probably due to slightly higher value of the blockage factor.

The magnetic field clearly influences the formation of a uniform velocity field in all sections shown, at small Reynolds numbers and at higher values of Hartmann number the velocity field becomes uniform at a very small distance behind the bluff body.

Figure 5 shows the results obtained experimentally and numerically in the case of the smooth sphere with a Re = 16000. There is a slight disturbance of the fluid-flow and velocity field in the cross-sections in front of the sphere, because of the relation of inertia and viscous forces. On the other hand, the influence of the magnetic field for the same values of Hartmann number becomes smaller. The velocity field behind the smooth sphere is not uniform, and the stream is diverted in a direction transverse to the effect of the magnetic field, last graph in fig. 5.

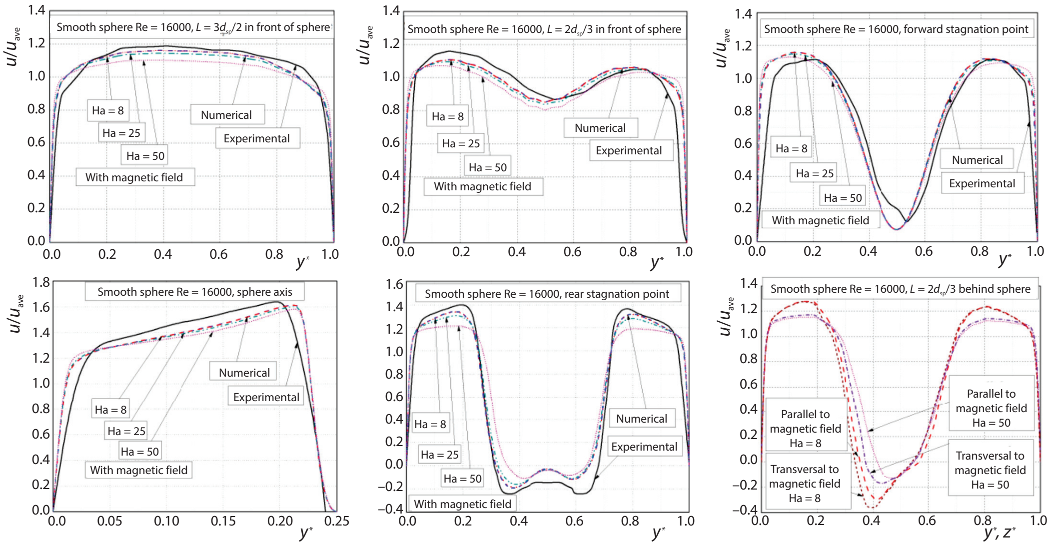

Figure 5. Comparison of velocity profiles for flow around the smooth sphere (Re = 16000)

Further, the results obtained experimentally and numerically for the velocity field around the sphere with dimples are presented. The results for Re = 1000 are presented first, fig. 6.

Here is also noticeable *more laminar* velocity profile obtained by measurements. But it is also important to notice the influence of the dimpled sphere on the velocity field, that becomes slightly wavy in the intersections in front of the sphere, which is not monitored numerically. The influence of the dimpled sphere on the incoming fluid-flow is certainly greater than numerically obtained. In this case numerical simulation does not reflect the velocity field in the

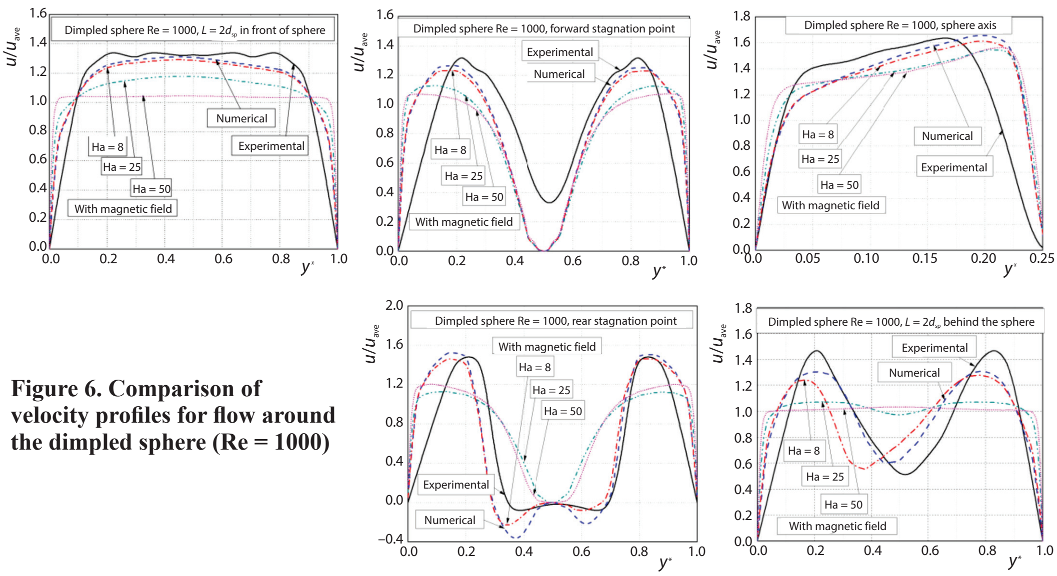

Figure 6. Comparison of velocity profiles for flow around the dimpled sphere (Re = 1000)

best manner, and it can be concluded that numerical results shows a slightly higher uniformity of the velocity profile.

The experimental results show a slightly higher disturbance of the flow compared to the numerical results. In the case of a sphere with dimples, a larger distance behind the sphere is required to obtain the uniform velocity field by using a magnetic field.

The observation is that lower intensity of the magnetic field shows better agreement with experimental results at this Reynolds number and blockage factor. It seems that flow models in CFD analysis and smaller Reynolds numbers give results that are closer to fully developed turbulent flow.

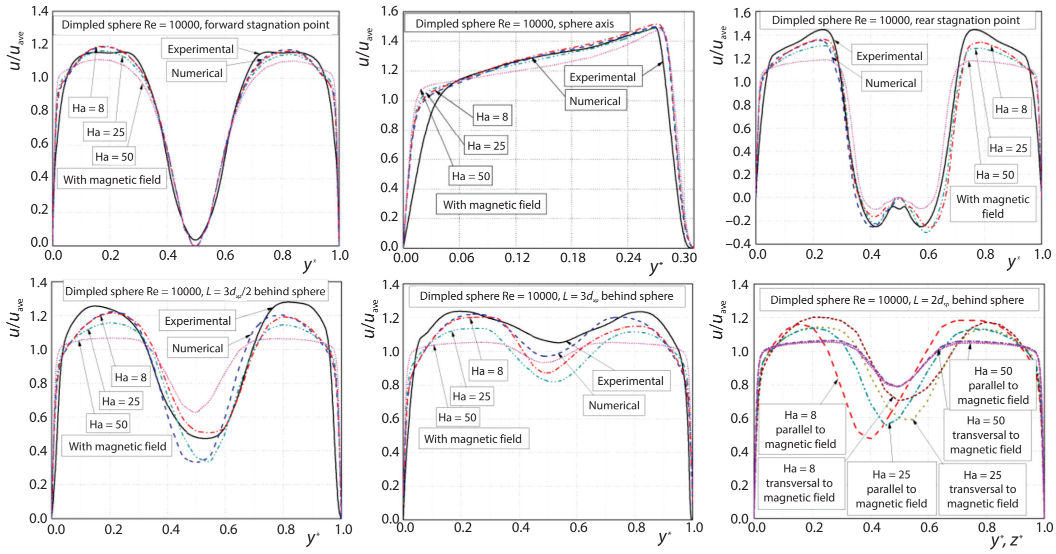

Figure 7. Comparison of velocity profiles for flow around the dimpled sphere (Re = 10000)

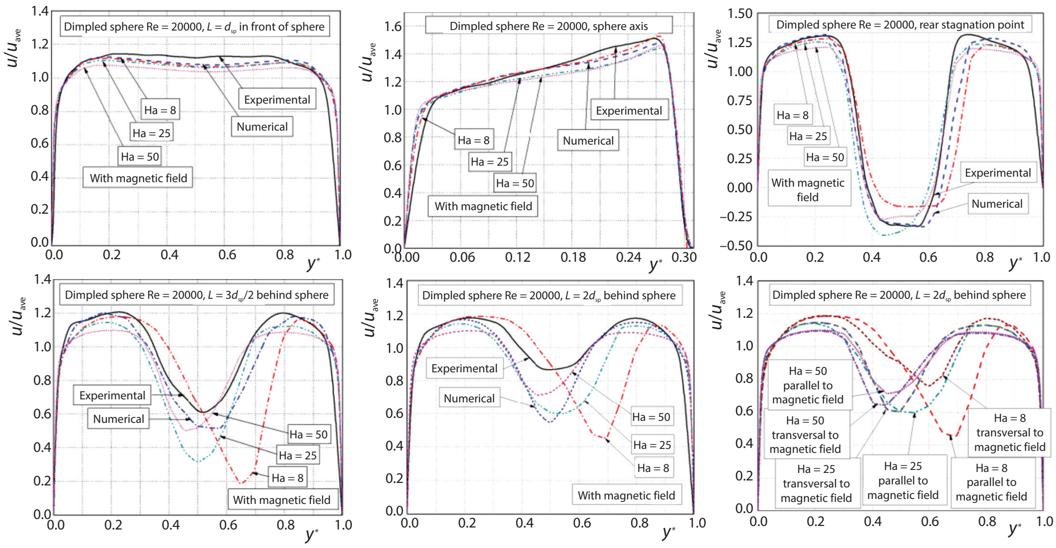

Figure 8. Comparison of velocity profiles for flow around the dimpled sphere (Re = 20000)

In addition the previously presented results, the flow around the dimpled sphere was analyzed for two more Reynolds numbers, and these results are shown in the following graphs. The results shown in fig. 7 and fig. 8 indicate significantly better agreement between experimental and numerical results for larger Reynolds numbers.

The influence of the magnetic field is also clearly observed, but it is much smaller than for the previous flow regime. It is important to note that there is a deflection of flow behind the sphere in the case of a magnetic field, but since the conductivity of the channel walls is not considered (*i.e.*, they were considered non-conductive), the flow deflection at smaller values of Hartmann number occurs in both directions perpendicular to the main flow direction.

As mentioned earlier, the measurement of the 2-D Reynolds stress tensor of a quasi steady flow was made using a rotated 1-D probe instead of a 2-D LDA system, relying on earlier

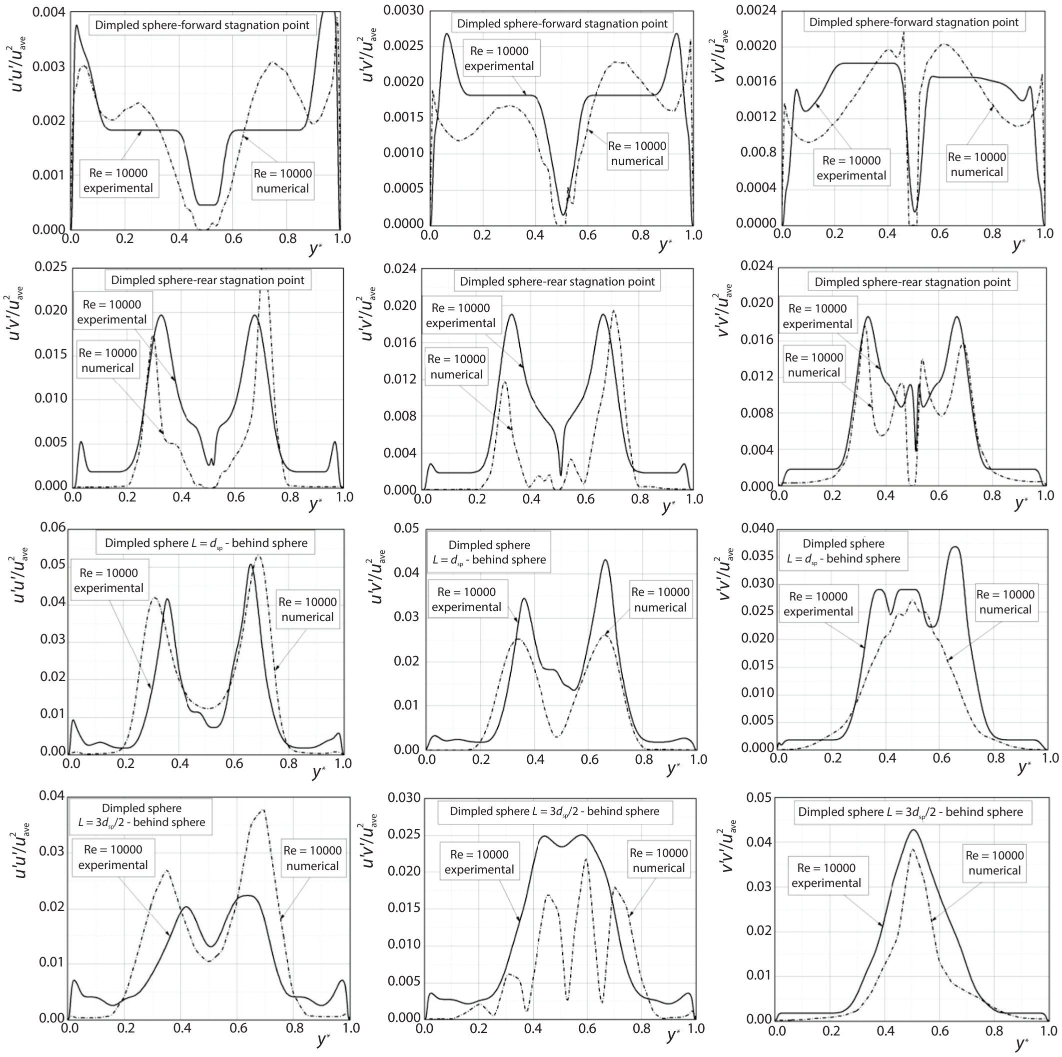

Figure 9. Sphere with dimples: comparison of LDA measurements and numerical simulations of Reynolds stresses components

investigations that showed very satisfactory results. Results of three Reynolds stresses components (u'^2, v'^2 and $u'v'$) are presented in fig. 9, for several measured cross-sections of the channel.

It certainly recognizes the almost complete identical tendency of all the results analyzed. Since the obtained values are small, the absolute error is large in some cases, but the consistent matching of the results for the fluctuating values is very satisfactory. It is also be noted that in this case, the experimental results (determined in the manner which is previously described) are even more *stable* than numerical results.

The results related to the Reynolds stresses in the case of an existing magnetic field and its absence are shown in fig. 10. Data and measurements were analyzed for the plane, *i.e.* cross-section, parallel to the action of the magnetic field. For all the analyzed results, the same tendencies are observed, but also a significant decrease of the Reynolds stresses under the action of the magnetic field.

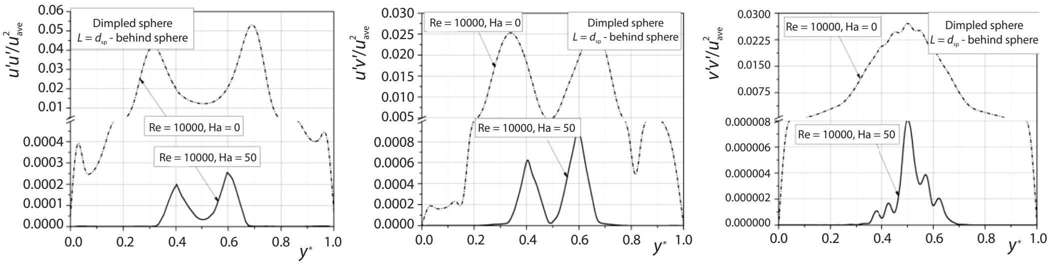

Figure 10. Sphere with dimples: comparison of LDA measurements and numerical simulations of Reynolds stresses components with magnetic field

In fig. 11 are shown the previously obtained results, which are now compared with the data obtained for the axis perpendicular to the effect of the magnetic field. It is noticeable a decrease of the velocity fluctuation components in the transverse direction, which is parallel with the magnetic field, while the velocity fluctuation component v in the z-axis is maintained the same or even increased.

Results related to the analysis of Reynolds stresses are obtained by using DES, where different time steps are analyzed during the unsteady flow regimes. Careful analysis has revealed that there are no significant deviations in numerically and experimentally obtained results. Certainly, as expected, there is a relatively symmetrical change of the flow image around the sphere, but this does not substantially change the obtained results, *i.e.* they are cyclically repetitive. On the other hand, one can clearly see the tendency of *quenching* the turbulent kinetic energy when there is a magnetic field and its fluctuation in the absence of a magnetic field, fig. 12.

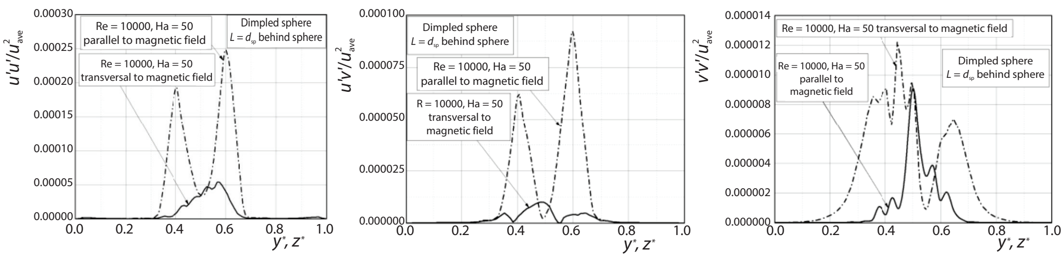

Figure 11. Sphere with dimples: comparison of Reynolds stresses components in parallel and transversal directions to the applied magnetic field

All the cases analyzed previously served to carry out some more analyzes that are presented in the function of Hartmann number. The effects of the Hartmann number on the drag and lift coefficients are shown in fig. 13. Two important facts are noted here. The drag coefficient, c_d, increases with the intensity of the applied magnetic field for the same Reynolds number both in the case of a smooth and a dimpled sphere. The increase in the drag coefficient is much larger with smaller Reynolds numbers, while with the increase of Reynolds number the increase of the drag coefficient disappears, even smaller values are obtained numerically. On the other hand, the lift coefficient, c_l, decreases with the increase of Hartmann number, but it is important to emphasize that at low intensities of a magnetic field and higher Reynolds number values this coefficient first increases, which may be relevant in technical practice.

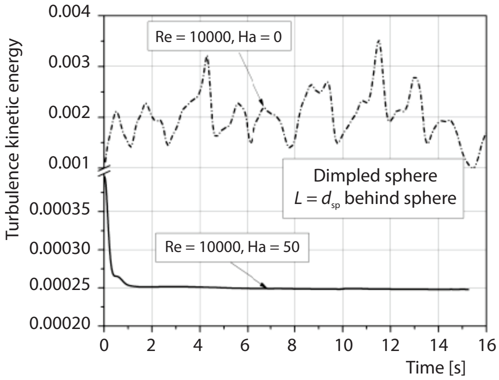

Figure 12. Sphere with dimples: Turbulent kinetic energy in case of absence and applied magnetic field

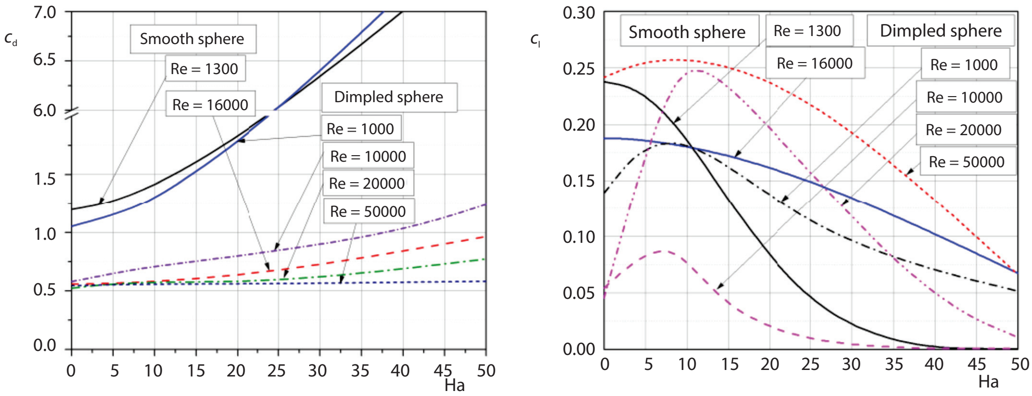

Figure 13. Drag coefficient for smooth and dimpled sphere, for different Reynolds and Hartmann's numbers

Figure 14 shows the results relating to the change in pressure coefficients, c_p, for different flow regimes (different Reynolds number) and different Hartmann's number. Higher absolute values of the pressure coefficient are obtained for larger Hartmann numbers and smaller Reynolds numbers. A significant change in the pressure coefficient occurs in the zone around half the sphere, both in the case of the smooth and dimpled sphere. With the increase of the Reynolds number, the change of the pressure coefficient is much smaller, despite the application of a higher intensity of the magnetic field (Ha = 50). Increasing the intensity of the magnetic field almost completely offsets the pressure coefficient in the other half of the sphere on both sides, while in the absence of a magnetic field it is clearly observed the uneven values of the pressure coefficient on the upper and lower side of the sphere (for angles larger than 90°).

Figure 15 shows the influence of the magnetic field on the position of the separation point. What is quite obvious is that an increase in the intensity of the magnetic field causes the delay of the boundary-layer separation. Also, for different flow regimes the results of separation point angles are presented in fig. 16. Higher values of Reynolds numbers require a higher

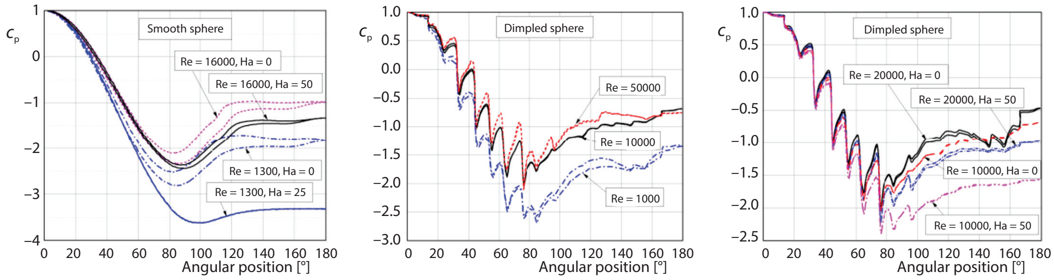

Figure 14. Pressure coefficient for smooth and dimpled spheres, for various Reynolds and Hartmann's numbers

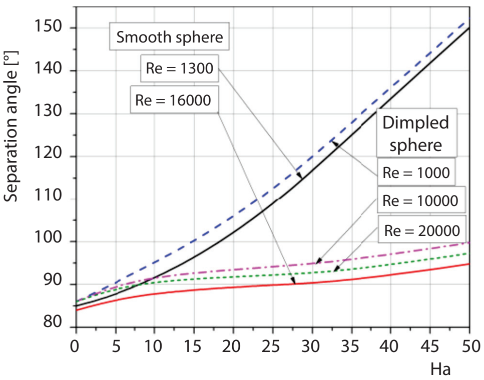

Figure 15. Separation point angle in function of Hartmann number for smooth and dimpled spheres

intensity of the magnetic field to delay the separation point, while at smaller values of Reynolds numbers it is possible to lead to almost complete absence of boundary-layer separation.

Figure 16 shows the boundary-layer separation zones for flow around smooth and dimpled spheres, where the first column of images corresponds to the absence of a magnetic field, while the second, third and fourth columns correspond to Hartmann's numbers 8, 25, and 50, respectively. The first row refers to the smooth sphere and Reynolds number 1300, while the second row of figures corresponds to the Reynolds number 16000. The third and fourth rows refer to the sphere with dimples and Reynolds numbers 1000 and 10000, respectively.

At the very end of this analysis, based on unsteady CFD simulations, the occurrence of vortex shedding and the influence of the magnetic field on this phenomenon are discussed. More detailed analysis concerning the influence of the magnetic field on the development of turbulence is the subject of our further research. For now, the value of the Strouhal number is first confirmed on the models and the necessary duration of the numerical simulations is defined, in which it is possible to observe all phenomena of importance for consideration of the unsteady flow around the dimpled sphere. On the other hand, vortex shedding is obviously significantly reduced in the case of a magnetic field, and it can be clearly seen from the last column of fig. 17. Thus, the first four columns refer to the flow in the absence of a magnetic field, and the author's intention is to present the same moments of time and the same number of examples in the case of a magnetic field in order to make comparisons. After analyzing numerous numerical simulations for Hartmann's number equal to 50 and Reynolds's number 10000, it was determined that there was no significant change in the flow field and the vortex shedding. And as mentioned before, it will be the subject of further research.

Conclusion

In this paper, the problems of flow around a smooth and dimpled sphere are analyzed experimentally and numerically, considering also the influence of the added magnetic field. In addition measuring the velocity field around the sphere and comparing the results with the numerical results obtained using the ANSYS-CFX software, LDA measurements of Reynolds stresses were

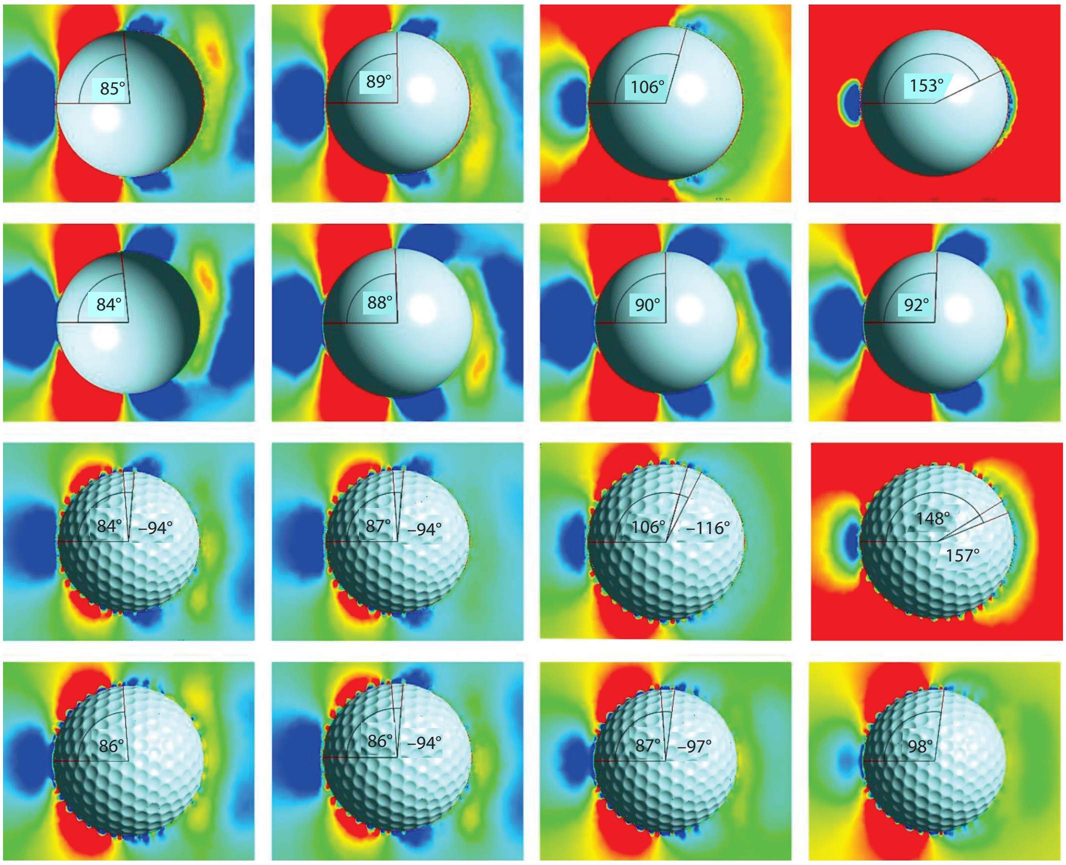

Figure 16. Separation point angle in function of Hartmann number for smooth and dimpled spheres

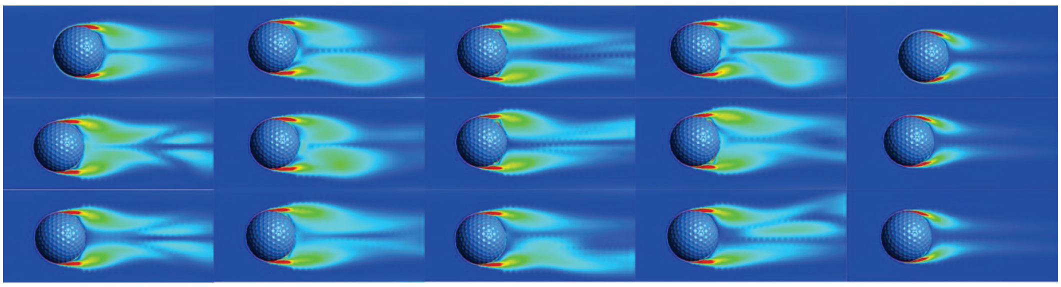

Figure 17. Vortex shedding in function of Hartmann number for the dimpled sphere

also performed. The obtained experimental results are compared with numerical simulations, giving a general conclusion that all analyzed results of all flow regimes are in a very good agreement. Experimental results indicate *more laminar* velocity profile, probably due to slightly higher value of the blockage factor. From all obtained results presented on numerous graphs, the effects of viscous, inertial and Lorentz forces are very noticeable, which is clearly indicated in the analysis of the results. A larger effect of the dimpled sphere on incoming flow was also determined experimentally, which was not observed in CFD simulations. This problem needs to be investigated in more detail. It has been shown that very satisfactory results can be obtained with measurements of the 2-D Reynolds stress tensor of a quasi steady flow by using a rotated 1-D LDA probe. Quasi static DES simulation shows that with a slightly stronger magnetic field, turbulence is nearly completely suppressed. The effect of magnetic field on the suppression of turbulence by the magnetic field can be observed from the instantaneous cross-sectional distribution of Reynolds stress tensor components and also absence of vortex shedding behind spheres.

Acknowledgment

This research was financially supported by the Ministry of Education, Science and Technological Development of the Republic of Serbia.

References

[1] Coutanceau, M., Bouard, R., Experimental Determination of the Main Features of the Viscous Flow in the Wake of a Circular Cylinder in Uniform Translation – Part 1: Steady Flow, *Journal Fluid Mech.*, *79* (1977), 2, pp. 231-256
[2] Cliffe, K. A., Tavener, S. J., The Effect of Cylinder Rotation and Blockage Ratio on the Onset of Periodic Flows, *Journal Fluid Mech.*, *501* (2004), Feb., pp. 125-133
[3] Behr, M., *et al.*, Incompressible Flow Past a Circular Cylinder: Dependence of the Computed Flow Field on the Location of the Lateral Boundaries, *Comput. Meth. Appl. Mech. Eng.*, *123* (1995), 1-4, pp. 309-316
[4] Zovatto, L., Pedrizzetti, G., Flow about a Circular Cylinder between Parallel Walls, *Journal Fluid Mech.*, *440* (2001), Aug., pp. 1-25
[5] Anagnostopoulos, P., *et al.*, Numerical Study of the Blockage Effects on Viscous Flow Past a Circular Cylinder, *Int. J. Numer. Meth. Fluids*, *22* (1996), 22, pp. 1061-1074
[6] Sahin, M., Owens, R. G., A Numerical Investigation of Wall Effects up to High Blockage Ratios on 2-D Flow Past a Confined Circular Cylinder, *Phys. Fluids*, *16* (2004), 5, pp. 1305-1320
[7] Bakic, V., *et al.*, Experimental Investigation of Turbulent Structures of Flow Around a Sphere, *Thermal Science*, *10* (2006), 2, pp. 97-112
[8] Haverkort, J. W., Peeters, T. W., JMagnetohydrodynamics of Insulating Spheres, Magnetohydrodynamics, *45* (2009), 1, pp. 111-126
[9] Dousset, V., Potherat, A., Numerical Simulations of a Cylinder Wake under a Strong Axial Magnetic Field, *Phys. Fluids*, *20* (2008), 20, 017104
[10] Muck, B., *et al.*, The 3-D MHD Flows in Rectangular Ducts with Internal Obstacles, *Journal Fluid Mech.*, *418* (2000), Sept., pp. 265-295
[11] Frank, M., *et al.*, Visual Analysis of 2-D Magnetohydrodynamics, *Phys. Fluids*, *13* (2001), 8, pp. 2287-2295
[12] Alboussiere, T., *et al.*, Quasi-2d MHD Turbulent Shear Layers, *Exp. Therm. Fluid Sci.*, *20* (1999), 20, pp. 19-24
[13] Kolesnikov, Y. B., Tsinober, A. B., Experimental Investigation of 2-D Turbulence behind a Grid, *Fluid Dyn.*, *9* (1974), 9, pp. 621-624
[14] Moreau, J., Sommeria, R., Electrically Driven Vortices in a Strong Magnetic Field, *Journal Fluid Mech.*, *189* (1988), Apr., pp. 553-569
[15] Dearing, S. S., *et al.*, Flow Control with Active Dimples, *The Aeronautical Journal*, *111* (2007), 1125, pp. 705-714
[16] Lienhart, H., *et al.*, Drag Reduction by Dimples, A Complementary Experimental/Numerical Investigation, *Int. J. Heat Fluid-Flow*, *29* (2008), 3, pp. 783-791
[17] Luo, Y. H., *et al.*, Advances of Drag-Reducing Surface Technologies in Turbulence Based on Boundary-Layer Control, *Journal Hydrodyn.*, *27* (2015), 4, pp. 473-487
[18] Ge, M., *et al.*, Drag Reduction of Wall Bounded Incompressible Turbulent Flow Based on Active Dimples/Pimples, *Journal Hydrodyn*, *29* (2017), 2, pp. 261-271
[19] Bogdanovic-Jovanovic, J., *et al.*, Experimental and Numerical Investigation of Flow Around a Sphere with Dimples for Various Flow Regime, *Thermal Science*, *16* (2012), 4, pp. 1013-1026
[20] Stieger, R. D., Hodson, H. P., Reynolds Stress Measurement with a Single Component Laser-Doppler Anemometer, *Proceedings*, 16th Symposium on Measuring Techniques in Transonic and Supersonic Flow in Cascades and Turbomachines, Cambridge, UK, 2002

Paper submitted: April 30, 2020
Paper revised: May 24, 2020
Paper accepted: May 29, 2020